PNAS RESEARCH ARTICLE | CELL BIOLOGY OPEN ACCESS

Nuclear speckle integrity and function require TAO2 kinase

Shengyan Gao[a], Matthew Esparza[a], Ishmael Dehghan[b,c], Vasilisa Aksenova[d], Ke Zhang[a], Kimberly Batten[a], Max B. Ferretti[e], Bridget E. Begg[e], Tolga Cagatay[a], Jerry W. Shay[a], Adolfo García-Sastre[f,g,h,i,j], Elizabeth J. Goldsmith[k], Zhijian J. Chen[b,c], Mary Dasso[d], Kristen W. Lynch[e], Melanie H. Cobb[l,1], and Beatriz M. A. Fontoura[a,1]

Contributed by Melanie H. Cobb; received April 6, 2022; accepted May 16, 2022; reviewed by Maximiliano D'Angelo and Michael Rout

Nuclear speckles are non–membrane-bound organelles known as storage sites for messenger RNA (mRNA) processing and splicing factors. More recently, nuclear speckles have also been implicated in splicing and export of a subset of mRNAs, including the influenza virus M mRNA that encodes proteins required for viral entry, trafficking, and budding. However, little is known about how nuclear speckles are assembled or regulated. Here, we uncovered a role for the cellular protein kinase TAO2 as a constituent of nuclear speckles and as a factor required for the integrity of these nuclear bodies and for their functions in pre-mRNA splicing and trafficking. We found that a nuclear pool of TAO2 is localized at nuclear speckles and interacts with nuclear speckle factors involved in RNA splicing and nuclear export, including SRSF1 and Aly/Ref. Depletion of TAO2 or inhibition of its kinase activity disrupts nuclear speckle structure, decreasing the levels of several proteins involved in nuclear speckle assembly and splicing, including SC35 and SON. Consequently, splicing and nuclear export of influenza virus M mRNA were severely compromised and caused a disruption in the virus life cycle. In fact, low levels of TAO2 led to a decrease in viral protein levels and inhibited viral replication. Additionally, depletion or inhibition of TAO2 resulted in abnormal expression of a subset of mRNAs with key roles in viral replication and immunity. Together, these findings uncovered a function of TAO2 in nuclear speckle formation and function and revealed host requirements and vulnerabilities for influenza infection.

TAOK2 | nuclear speckles | splicing | mRNA export

Significance

In these studies, TAO2 kinase has been revealed as a constituent and key player in nuclear speckle structure and function, including RNA splicing and nuclear export. These findings add knowledge to the cell biology of nuclear body assembly, RNA processing, and influenza virus infection, as this human pathogen utilizes nuclear speckles for generating a spliced product that is critical for viral entry and budding. Thus, regulation of TAO2 activity may be considered a therapeutic strategy for targeting influenza virus.

The compartmentalization of the eukaryotic nucleus allows for the physical separation of functional activities and is closely linked to messenger RNA (mRNA) processing and maturation steps such as pre-mRNA splicing. We and others have shown that the splicing and trafficking of nascent transcripts in the nucleus are tightly regulated to control gene expression (1–3). However, despite decades of research, much remains to be learned about the regulators of RNA processing and nuclear architecture. Importantly, viruses often hijack compartmentalization and processing of nuclear RNA to promote the expression of their own genes; thus, the study of virus–host interactions has historically provided unexpected and critical insight into nuclear structure and function (2, 4, 5). Equally important to both viral and host mRNA processing are nuclear speckles, which are membraneless assemblies that are defined by puncta of nuclear staining with antibodies to the RNA-binding proteins SC35, SRRM2, or SON (6, 7). Nuclear speckles are typically considered to be storage sites for splicing factors that traffic to the nucleoplasm to splice most cellular pre-mRNAs (8, 9). However, there is evidence indicating that a subset of cellular mRNAs are posttranscriptionally spliced at nuclear speckles (10). Additionally, mRNA export factors are also enriched at nuclear speckles (11) and intronless mRNAs traffic through nuclear speckles for nuclear export (12).

We have shown that influenza virus usurps nuclear speckles to splice and export key viral mRNAs that encode proteins required for viral entry, trafficking, and budding (2). Influenza virus enters the cell via endocytosis, and the M2 proton channel present in the viral membrane allows acidification of the viral particle for uncoating and subsequent release of the eight viral genomic RNA segments (viral ribonucleoproteins or vRNPs) into the cytoplasm upon viral membrane fusion with the endosomal membrane (13). The vRNPs are then imported into the nucleus, where they are transcribed and replicated. Two of the vRNPs (M and NS) are transcribed into M1 and NS1 mRNAs and alternatively spliced into M2 and NS2 mRNAs, respectively. M1 can also be spliced into other less known isoforms. In addition to being spliced, M1 mRNA (unspliced) is also exported from the nucleus to be translated into M1 protein, which has a role in mediating vRNP nuclear export and viral assembly, forming a coat under the viral membrane (13). M2 mRNA encodes the M2 proton channel required for viral entry (13) and assembly (14, 15), and is also involved in autophagy (16). NS1 mRNA is translated into a major

Author contributions: S.G. and B.M.A.F. designed research; S.G., M.E., I.D., K.Z., M.B.F., B.E.B., and T.C. performed research; V.A., K.B., J.W.S., A.G.-S., E.J.G., Z.C., M.D., K.W.L., M.H.C., and B.M.A.F. contributed new reagents/analytic tools; S.G., M.E., I.D., K.Z., K.B., J.W.S., Z.C., K.W.L., M.H.C., and B.M.A.F. analyzed data; and S.G., A.G.-S., K.W.L., M.H.C., and B.M.A.F. wrote the paper.

Reviewers: M.D., Sanford Burnham Prebys Medical Discovery Institute; and M.R., The Rockefeller University.

Competing interest statement: The A.G.-S. laboratory has received research support from Pfizer, Senhwa Biosciences, Kenall Manufacturing, Avimex, Johnson & Johnson, Dynavax, 7Hills Pharma, Pharmamar, ImmunityBio, Accurius, Nanocomposix, Hexamer, N-fold LLC, Model Medicines, Atea Pharma, and Merck, outside of the reported work. A.G.-S. has consulting agreements with the following companies involving cash and/or stock: Vivaldi Biosciences, Contrafect, 7Hills Pharma, Avimex, Vaxalto, Pagoda, Accurius, Esperovax, Farmak, Applied Biological Laboratories, Pharmamar, Paratus, CureLab Oncology, CureLab Veterinary, Synairgen, and Pfizer, outside of the reported work. A.G.-S. has been an invited speaker at meeting events organized by Sequirus, Janssen, and AstraZeneca. A.G.-S. is an inventor on patents and patent applications on the use of antivirals and vaccines for the treatment and prevention of virus infections and cancer, owned by the Icahn School of Medicine at Mount Sinai, outside of the reported work.

[1]To whom correspondence may be addressed. Email: melanie.cobb@utsouthwestern.edu or beatriz.fontoura@utsouthwestern.edu.

This article contains supporting information online at http://www.pnas.org/lookup/suppl/doi:10.1073/pnas.2206046119/-/DCSupplemental.

Published June 15, 2022.

virulence factor, NS1 protein, that inhibits antiviral responses, and NS2 mRNA encodes the NS2 protein (NEP), which mediates vRNP nuclear export (13, 17). After transcribing and translating its mRNAs and replicating its genome, influenza virus genomic RNAs leave the nucleus and together with viral proteins assemble new virions that bud from the plasma membrane.

Recently, we identified small-molecule inhibitors of influenza virus M mRNA processing and nuclear export, which consequently impair virus replication (18). One of these inhibitors targets TAO2 (19). Full-length TAO2 is composed of an N-terminal kinase domain and a poorly characterized C terminus that is predicted to be partially disordered and to have long helices, which likely mediate protein–protein interactions. TAO2 was first studied as an activator of MAP2Ks 3, 4, and 6 of the stress-responsive mitogen-activated protein kinase pathways (20). Subsequently, TAO2, and its paralogs TAO1 and TAO3, have been implicated in a number of additional signaling pathways (21, 22), and TAO2 activity in neurons has recently been linked to behavior, cognitive abnormalities, and autism spectrum disorder (23–25). However, much about the localization and function of TAO2 in specific cellular compartments remains unknown.

Since we identified a chemical inhibitor of influenza virus M mRNA processing and nuclear export that targets TAO2 (18, 19), we sought to determine the intracellular localization of TAO2 and uncover its potential role in the influenza virus life cycle. Here, we show that a significant pool of TAO2 is concentrated at nuclear speckles and demonstrate that TAO2 interacts with key splicing and other RNA-processing factors at these nuclear bodies. We also found that TAO2 is required for the integrity and function of nuclear speckles, including splicing and nuclear export of a subset of influenza virus mRNAs that are processed at nuclear speckles, such as M mRNAs. In addition, we show that TAO2 is critical for expression of a subset of cellular mRNAs, among which are mRNAs that encode factors with key functions in viral immunity. Indeed, we found that TAO2 supports influenza virus replication. Thus, these data demonstrate a role for TAO2 in nuclear speckle architecture and function and point to a potential effect of this cellular kinase in the regulation of both influenza virus replication and immunity.

Results and Discussion

We previously performed a high-throughput screen to identify chemical inhibitors of influenza virus M mRNA export (18), a process that occurs via nuclear speckles where a pool of M1 mRNA is spliced into M2 mRNA prior to nuclear export (2). Among the identified hits was a known TAO2 kinase inhibitor (19). This finding led us to further investigate the intracellular localization of TAO2. Interestingly, using a polyclonal rabbit anti-TAO2 antibody raised previously against a peptide antigen that is not shared by TAO1 or 3 (20), we found a substantial intranuclear pool of TAO2 at nuclear speckles as it colocalized with the nuclear speckle marker SC35 (Fig. 1*A*). To then assess the function of TAO2 with respect to these intranuclear bodies, we knocked down TAO2 with small interfering RNAs (siRNAs) and found that TAO2 depletion reduced the amount and speckle

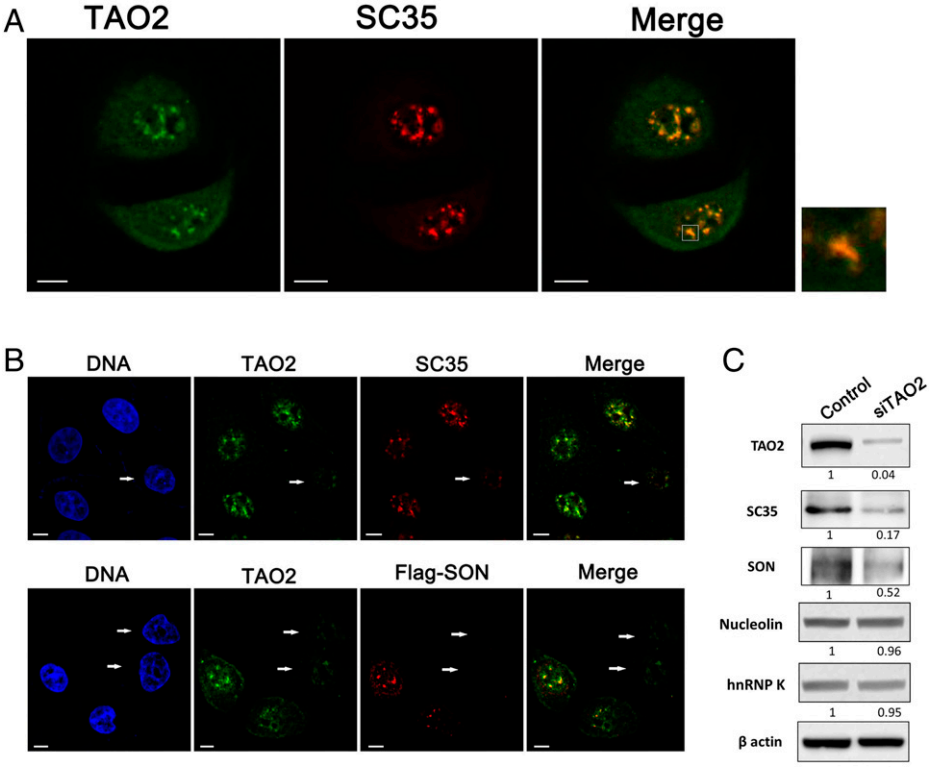

Fig. 1. TAO2 is localized at nuclear speckles and maintains the basal levels of nuclear speckle factors. (*A*) A549 cells were subjected to immunofluorescence microscopy with rabbit anti-TAO2 serum and mouse SC35 antibody. The enlarged image on the right depicts a nuclear speckle from the merge panel (marked region). (Scale bars, 5 μm.) $n = 3$. (*B*) A549 cells or A549 cells with the SON gene tagged with Flag, HA, and AID were transfected with control siRNA or with an siRNA pool targeting TAO2 and then subjected to immunofluorescence microscopy with antibodies against TAO2 and SC35, or with anti-FLAG antibodies to detect SON protein. White arrows indicate cells with decreased levels of TAO2 compared with neighboring cells. (Scale bars, 5 μm.) (*C*) A549 cells were transfected with control siRNA or siRNAs targeting TAO2, and whole-cell lysates were subjected to Western blot to detect endogenous TAO2, SC35, SON, nucleolin, and hnRNP K protein levels. β-actin serves as loading control. $n = 3$. The intensity of each protein band was quantified and normalized to β-actin levels.

localization of key nuclear speckle assembly and splicing factors—SON and SC35 (Fig. 1 *B* and *C*). Since a pool of heterogeneous nuclear RNP (hnRNP) K is also found at nuclear speckles (2), we assessed its levels upon TAO2 knockdown and found no significant changes (Fig. 1*C*). Similarly, we found no alterations in nucleolin levels (Fig. 1*C*), which is a known nucleolar marker, indicating that TAO2 is not inducing a more widespread effect on nuclear bodies but is specifically targeting nuclear speckles where it resides. To then determine whether the kinase activity of TAO2 is involved in this process, we used our TAO2 kinase inhibitor to test its impact on nuclear speckles. We found that inhibition of TAO2 kinase activity altered nuclear speckle shape and decreased the levels of SC35 (*SI Appendix*, Fig. S1), phenocopying TAO2 depletion. These results suggest that the kinase activity of TAO2 indeed has a role in nuclear speckle integrity.

To further understand the role of TAO2 in the nucleus, we have immunoprecipitated TAO2 from nuclear extracts of A549 cells and carried out mass spectrometry analysis. Notably, many TAO2-interacting partners identified in this assay (Fig. 2*A* and Dataset S1) overlap with proteins determined to be within the nuclear speckles in a recent study using a modified protocol of tyramide signal amplification mass spectrometry (26). Several of these TAO2- and speckle-associated proteins are also known splicing and mRNA export factors (Fig. 2*A*). Some of these factors identified as TAO2-interacting partners were further confirmed by immunoprecipitation of TAO2 from cell extracts, in the presence of RNasin or RNase A, followed by Western blot analysis. The splicing factor SRSF1 and the mRNA export factor Aly/Ref interacted with TAO2 in the presence and absence of RNA (Fig. 2*B*). SRSF1 plays a critical role in promoting assembly of the spliceosome to properly process pre-mRNAs (27) and Aly/Ref is a key adaptor protein for recruiting the major mRNA export receptor NXF1-NXT1 (28), which then docks the mRNA to the nuclear pore complex for export to the cytoplasm. Additionally, TAO2 depletion decreased the levels of both SRSF1 and Aly/Ref, indicating a critical role for TAO2 in maintaining the basal levels of these splicing and mRNA export factors (Fig. 2*C*). In sum, both our biochemical and imaging results corroborate the conclusion that TAO2 is present in, and involved in the formation of, nuclear speckles.

To determine if the interaction of TAO2 with factors critical for RNA processing and export indeed occurs at nuclear speckles in situ, we performed proximity ligation assays (PLAs) with antibodies against TAO2 and SRSF1. PLA was also performed using antibodies against TAO2 and NXF1 as a negative control. As shown in Fig. 3 *A* and *B*, PLA signals (red dots) were not observed when TAO2 and SRSF1 antibodies were used alone or in the presence of both TAO2 and NXF1 antibodies. These results demonstrated the lack of nonspecific signals in the presence of these antibodies. However, consistent with the biochemical interaction identified above (Fig. 2), PLA signals were detected when we combined TAO2 and SRSF1 antibodies (Fig. 3 *A* and *B*). We then further developed the PLA in combination with immunofluorescence microscopy to co-stain nuclear speckles with the SC35 antibody. In this manner, we could assess whether TAO2 interaction with SRSF1 occurs at nuclear speckles. As shown in Fig. 3 *C* and *D*, a significant percentage of the intranuclear PLA signal derived from the interaction between TAO2 and SRSF1 (42%) was indeed localized at nuclear speckles. Three-dimensional (3D) projection of PLA signals and nuclear speckles showed that this TAO2-SRSF1 pool is localized at the periphery of nuclear speckles (Fig. 3*D*). These results further corroborate TAO2 localization and interaction with constituents of nuclear speckles.

Our findings on TAO2 localization at nuclear speckles and interaction with splicing factors led us to test its potential role in regulating splicing of influenza virus M mRNA, which occurs at nuclear speckles (2). Influenza virus M1 mRNA is spliced into M2 mRNA at nuclear speckles while NS1-to-NS2 mRNA splicing likely occurs in the nucleoplasm, as we previously reported (2). To test the effect of TAO2 on M1 to M2 levels and splicing (Fig. 4*A*), we knocked down TAO2 (Fig. 4 *B* and *C*) and first assessed the levels of M1, M2, NS1, and NS2 mRNAs by quantitative real-time PCR (qPCR). We observed a decrease in the total amounts of these mRNAs (Fig. 4*D*). Additionally, the ratio of M2/M1 was reduced (Fig. 4*E*) while the ratio of NS2/NS1 was not altered (Fig. 4*F*), suggesting that M1-to-M2 splicing was impaired upon TAO2 depletion while NS1-to-NS2 splicing was not affected. Together, these results indicate that TAO2 is required for generating M and NS mRNAs as well as for M1-to-M2 splicing. Since M1-to-M2 splicing occurs at nuclear speckles, this finding suggests a functional disruption of nuclear speckles. This is consistent with the decrease in nuclear speckle proteins involved in splicing upon TAO2 knockdown, as well as the observed alteration in nuclear speckle structure under this condition (Fig. 1 *B* and *C*).

Since the next step after splicing is nuclear export (2), we have also assessed nucleocytoplasmic distribution of M mRNA upon depletion of TAO2 followed by single-molecule RNA–fluorescence in situ hybridization (smRNA-FISH) to detect M1 and M2 mRNAs. We show that TAO2 knockdown led to a significant retention of M mRNAs in the nucleus (Fig. 4*G*). This mRNA export inhibition was quantified and the intracellular distribution of the M1 mRNA fluorescence intensity was calculated in the nucleus (N) and in the cytoplasm (C), and then expressed as the N/C ratio. A higher N/C ratio of M mRNAs was observed in TAO2-depleted cells than in control cells (Fig. 4*H*), indicating mRNA export inhibition. In contrast, the intracellular distribution of NS1 and hemagglutinin (HA) mRNAs was not altered by TAO2 knockdown (*SI Appendix*, Fig. S2). This finding corroborates previous data showing that the NS1-to-NS2 mRNA splicing and export do not appear to occur via nuclear speckles and that NS1-to-NS2 splicing does not require NS1-BP, which is a key mediator of M mRNA splicing and export (2, 29, 30). Thus, both splicing and nuclear export of M mRNAs through nuclear speckles rely on TAO2 function. These findings are consistent with changes in nuclear speckle structure and composition observed upon TAO2 knockdown, which includes the reduced levels of the splicing factor SRSF1 and the mRNA export factor Aly/Ref. In fact, we have shown that Aly/Ref is a key mRNA export factor for M mRNAs (2).

To determine the impact of TAO2 depletion on influenza virus replication, we measured viral protein levels and viral replication in control versus TAO2-depleted cells. We found that TAO2 knockdown decreased the levels of influenza virus proteins (Fig. 5*A*) and inhibited viral replication (Fig. 5 *B* and *C*). This effect may be partially due to the disruption of nuclear speckle structure upon TAO2 knockdown that results in reduced M1-to-M2 splicing and nuclear export. As a consequence, the M2/M1 protein ratio is reduced and M2 protein function in viral entry, budding, and autophagy would be compromised. In fact, influenza virus replication is also inhibited upon knockdown of the nuclear speckle assembly/splicing factor SON protein (Fig. 5 *B* and *C*), as previously reported (2, 31). The extent of inhibition is similar to what we observed upon TAO2 knockdown (Fig. 5 *B* and *C*). Additionally, the decrease in TAO2 in the cytoplasm may down-regulate MAPK signaling (20), whose inhibition is known to prevent influenza

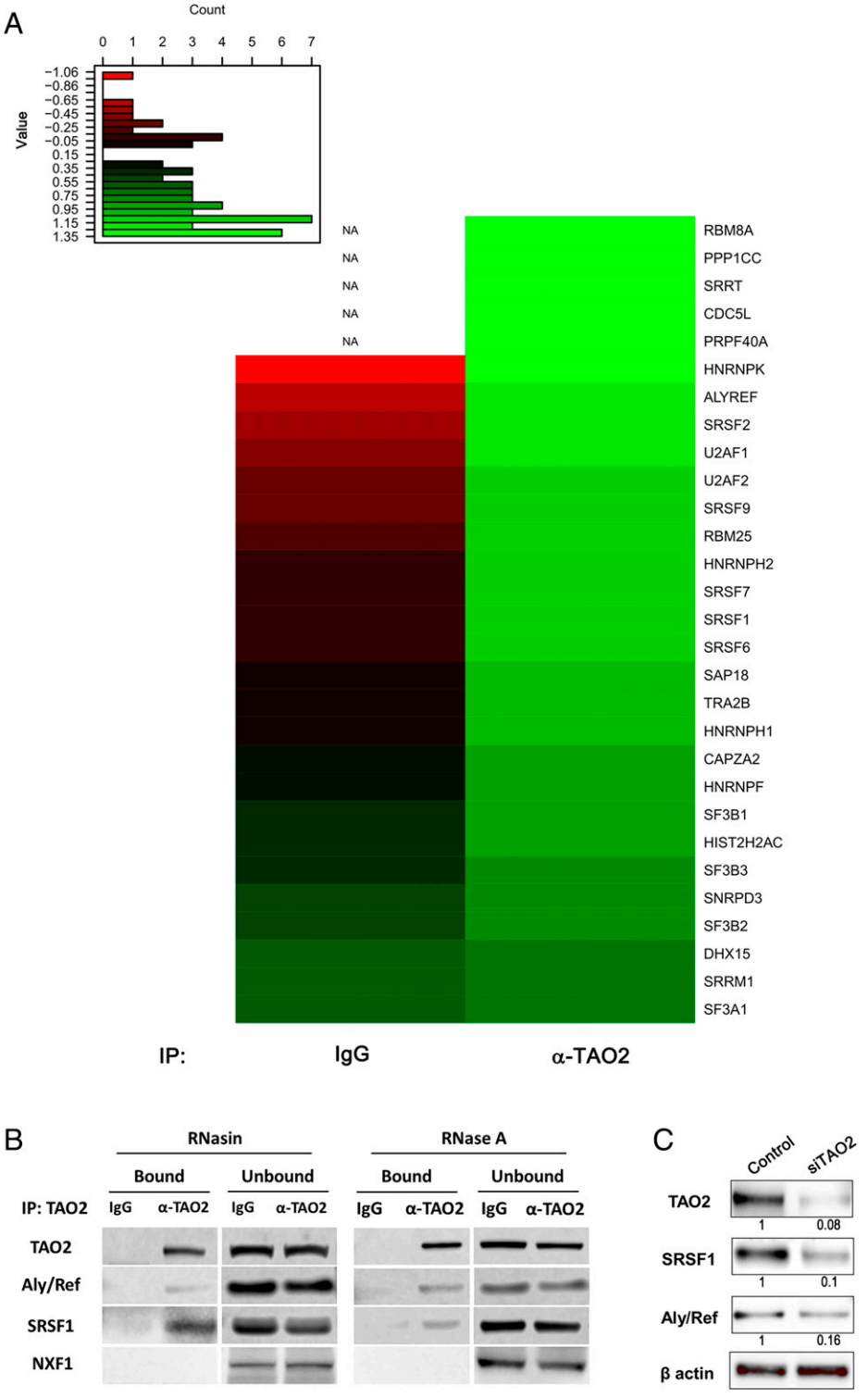

Fig. 2. Nuclear speckle proteome is associated with TAO2. Nuclear lysates from A549 cells were subjected to immunoprecipitation with control rabbit IgG or TAO2 antibody. (*A*) TAO2-interacting proteins were identified by mass spectrometry. The heatmap shows relative abundances of selected hits representing proteins that overlap with constituents of nuclear speckles. Control immunoprecipitation (IP) with IgG is compared with immunoprecipitation performed with TAO2 antibody. NA represents hits not detected in IgG-immunoprecipitated samples. (*B*) Immunoprecipitates were probed with the indicated antibodies to confirm the interactions between TAO2 and selected hits in *A*. NXF1 is used as negative control since it did not interact with TAO2 in the mass spectrometry analysis. $n = 3$. (*C*) A549 cells were transfected with control siRNA or siRNAs targeting TAO2, and whole-cell lysates were subjected to Western blot to detect endogenous TAO2, SRSF1, and Aly/Ref. β-actin serves as loading control. $n = 3$.

virus replication (32) and therefore may also contribute to the overall inhibition of viral replication observed upon TAO2 knockdown.

To test a potential effect of TAO2 on immune-regulated genes, we performed RNA-sequencing (RNA-seq) analysis of control versus TAO2-depleted cells in the absence of infection. We found that the levels of only a subset of cellular mRNAs were altered by TAO2 knockdown (Fig. 5*D*). Within this subset were up-regulated mRNAs that encode mediators of antiviral immunity such as the interferon-regulated MX1, OAS2,

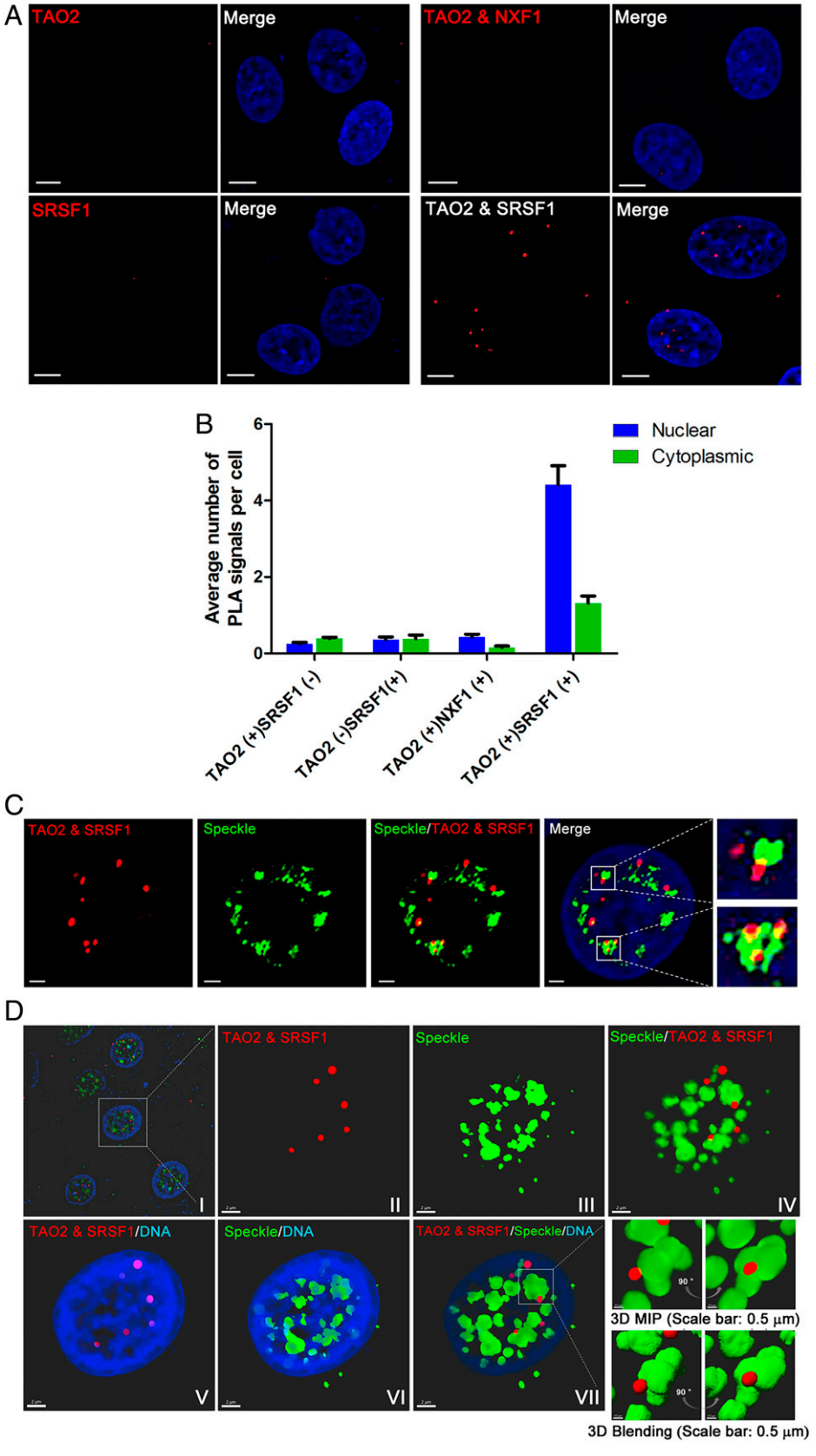

Fig. 3. Pool of the TAO2–SRSF1 complex is localized at the periphery of nuclear speckles. (*A*) A549 cells grown on coverslips were fixed and subjected to PLAs with the indicated primary antibodies. (Scale bars, 5 μm.) (*B*) PLA signals were quantified in 100 cells for each condition. Values are means ± SD. $n = 3$. (*C* and *D*) A549 cells were subjected to PLA to detect the TAO2–SRSF1 complex followed by immunofluorescence microscopy to stain nuclear speckles with an antibody against SC35. $n = 3$. (*C*) Two-dimensional images of PLA signals merged with nuclear speckles and DNA. (Scale bars, 2 μm.) (*D*) Three-dimensional projection of PLA signals and nuclear speckles. (*I*) Low magnification of the maximum-intensity projection (MIP) is shown. PLA signal of the TAO2–SRSF1 complex (red), nuclear speckles (SC35, green), and chromatin (blue). (*II* and *III*) High magnification of the MIP surfaces is shown for PLA signal of the TAO2–SRSF1 complex (red) and nuclear speckles are stained in green. (Scale bars, 2 μm.) (*IV*) Pairwise merged surface created for PLA signal of the TAO2–SRSF1 complex (red) and nuclear speckles (green) is shown. (*V*–*VII*) Views of a chromatin merged surface created for (*V*) PLA signal of the TAO2–SRSF1 complex (red), (*VI*) nuclear speckles (green), and (*VII*) PLA signal of TAO2–SRSF1 (red) and nuclear speckles (green) are shown. (Scale bars, 2 μm.) The squared marked area in *VII* is enlarged and shown in the view of 3D isometric MIP-rendering volume (*Top*) or 3D isometric blend-rendering volume (*Bottom*). Both 3D rendered volumes are presented in 90° alternative views to provide visual and spatial emphasis for the colocalization (yellow) of the TAO2–SRSF1 complex (red) and nuclear speckles (green). To calculate the percentage of the TAO2–SRSF1 complex colocalization with nuclear speckles, 156 cells were analyzed and 42% of the PLA signal was found at nuclear speckles.

IFI6, IFI44, and IFIT1 proteins (33–35) (Fig. 5 *D*, *Inset* and Datasets S2 and S3), which may also contribute to the inhibition of virus replication observed upon TAO2 knockdown (Fig. 5 *A*–*C*). Similar to TAO2 depletion, these interferon-regulated mRNAs were also up-regulated upon inhibition of TAO2 kinase activity (*SI Appendix*, Fig. S3), suggesting that the kinase activity is involved in this immune-regulatory process. Moreover, gene set enrichment analysis of the Kyoto Encyclopedia of Genes and Genomes (KEGG) database shows pathways that are regulated during infections by influenza virus,

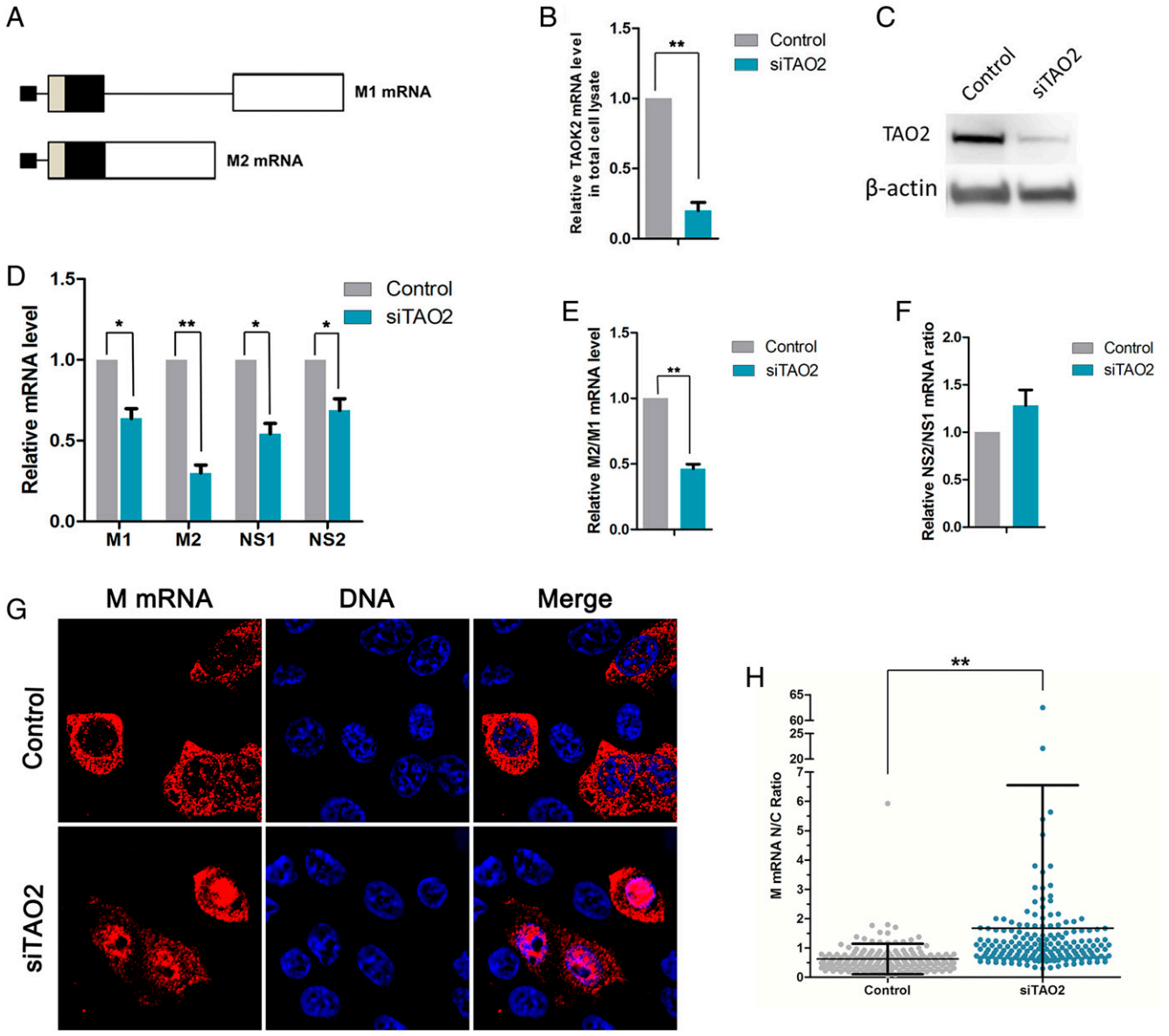

Fig. 4. Partial depletion of TAO2 impairs splicing and nuclear export of influenza virus M mRNA. (*A*) Schematic representation of influenza virus M1 and M2 mRNAs. Boxes denote exons and the line denotes an intron. (*B–F*) A549 cells were treated with control siRNA or siRNAs targeting TAO2 followed by infection with WSN at an MOI of 2 for 8 h. (*B*) Purified RNA from total cell lysates was subjected to qPCR to measure TAO2 mRNA. (*C*) Total cell lysates were subjected to Western blot to detect TAO2 protein levels. β-actin serves as loading control. $n = 3$. (*D*) Purified RNA from total cell lysates was subjected to qPCR to measure M1, M2, NS1, and NS2 mRNA levels. (*E* and *F*) The ratios of M2/M1 (*E*) and NS2/NS1 (*F*) mRNA levels are shown. Graphs show mean ± SD. $n = 3$. *$P < 0.05$, **$P < 0.01$. (*G*) A549 cells were treated with control or siRNAs targeting TAO2 followed by infection with WSN at an MOI of 2 for 8 h. smRNA-FISH was performed to detect M mRNA. (*H*) Nuclear-to-cytoplasmic fluorescence intensity (N/C ratio) was quantified. Control, $n = 177$ cells; siTAO2, $n = 181$ cells. **$P < 0.01$.

SARS-CoV-2, Epstein–Barr virus, Kaposi sarcoma–associated herpesvirus, and human papilloma virus (Fig. 5*E*). In addition, mRNAs that encode constituents of cytokine pathways and the PI3K-AKT pathway are also enriched by TAO2 depletion and both pathways are known regulators of viral replication and viral-mediated apoptosis (36–38). These putative TAO2 functions in infection and immunity may also be related to its interaction with SRSF1. It has been shown that SRSF1 is required for regulatory T cell functions that prevent autoimmunity (39) and for limiting interferon-gamma production (40). These processes would likely be impacted by modulation of TAO2 activity, which controls SRSF1 basal levels (Fig. 2*C*).

In sum, TAO2 is a constituent and key mediator and/or regulator of nuclear speckle assembly and function. As a result, TAO2 promotes expression of influenza virus M mRNAs, which usurp nuclear speckles for splicing and nuclear export. Furthermore, TAO2 alters expression of a subset of cellular mRNAs involved in viral infection and immunity. The latter processes likely include a combination of TAO2 functions in the nucleus and in the cytoplasm that ultimately result in the regulation of selective gene expression.

Materials and Methods

Cell Culture and Virus. Human lung adenocarcinoma epithelial (A549) cells were maintained in high-glucose Dulbecco's modified Eagle's medium (Gibco) supplemented with 10% fetal bovine serum (Sigma) and 100 U/mL penicillin/streptomycin antibiotics at 37 °C with 5% CO_2. Influenza virus (A/WSN/33) was propagated in Madin–Darby canine kidney cells and virus titer was determined by plaque assay, as previously described (41). A549 cells expressing 3×Flag-HA-AID-SON were generated using CRISPR-Cas9–mediated recombination, as previously described (42). Briefly, both alleles of the SON gene were tagged sequentially. The first allele was

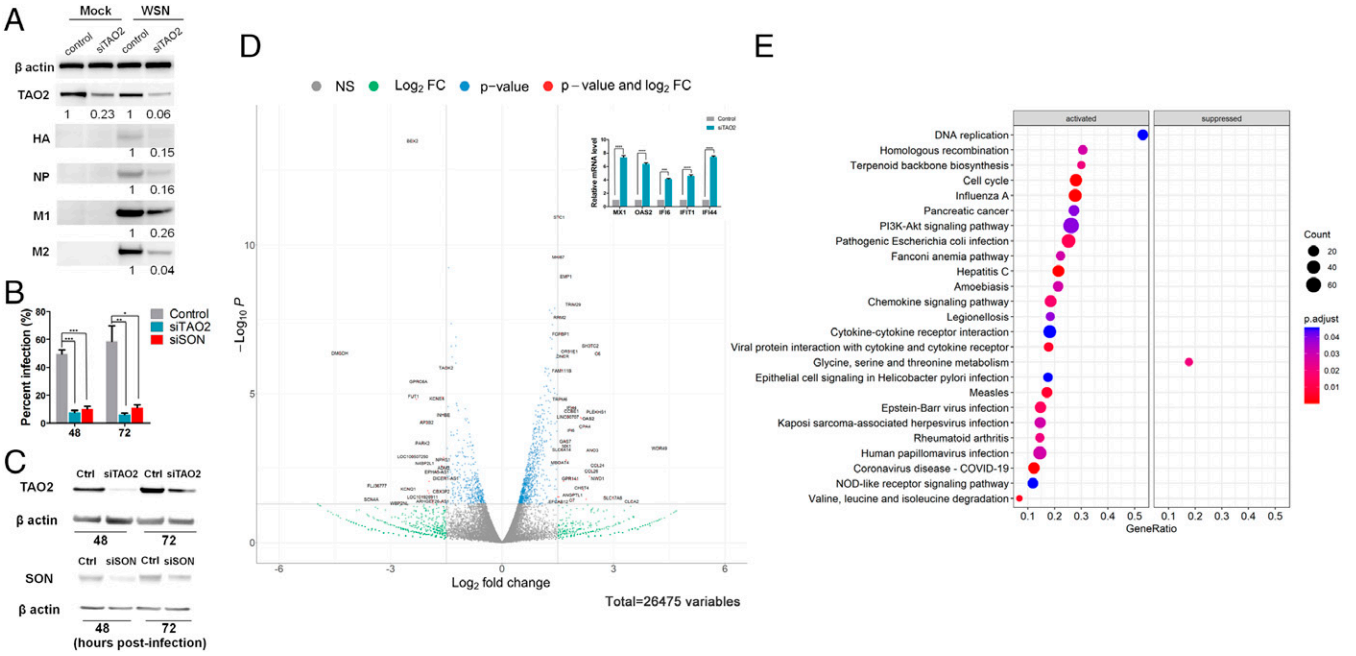

Fig. 5. Partial depletion of TAO2 results in inhibition of influenza virus replication and alters the levels of a subset of cellular mRNAs. (*A*) A549 cells were transfected with control siRNA or siRNAs targeting TAO2 followed by infection with WSN at an MOI of 2 for 8 h. Total cell lysates were subjected to Western blot to detect the levels of β-actin (loading control), TAO2, and viral proteins HA, NP, M1, and M2. (*B* and *C*) Cells were infected with WSN at an MOI of 0.01 and supernatants and cell lysates were collected at the indicated time points after infection. (*B*) Supernatants were used in viral replication assays following NP expression. (*C*) Cell lysates were subjected to Western blot analysis to assess the levels of TAO2, SON, and β-actin (loading control). (*D*) Depletion of TAO2 alters the levels of a subset of cellular mRNAs. Total mRNA from cells treated with control siRNA or siRNAs targeting TAO2 was subjected to RNA-seq analysis. The volcano plot depicts total levels of individual cellular mRNAs upon TAO2 knockdown. NS, not signficantly changed; FC, fold change. (*D*, *Inset*) Selected interferon-regulated mRNAs whose levels were up-regulated upon TAO2 knockdown, measured by qPCR. Graphs show means ± SD. $*P < 0.05$, $**P < 0.01$, $***P < 0.001$, $****P < 0.0001$. $n = 3$. (*E*) Gene set enrichment analysis of the KEGG database shows enrichment in pathways involved in the regulation of viral infections upon TAO2 depletion.

tagged with the 3×Flag tag, full-length 229–amino acid AID degron (flAID), and hygromycin AID gene. The second allele was tagged with the HA tag, a minimal functional 44–amino acid AID tag (1×microAID), and puromycin. The sequences of homology arms were amplified from genomic DNA extracted from a colorectal adenocarcinoma cell line (DLD-1). The sequence of E3 ubiquitin ligase TIR1 was integrated into the RCC1 locus, where RCC1 was tagged with an infrared fluorescent protein and a blasticidin resistance gene. In all cases, the selection marker was separated from the tagged gene by the sequence encoding self-cleavage peptide P2A.

Antibodies. TAO2 polyclonal antiserum (U2253) was generated as previously described (20). The antiserum was used at a 1:500 dilution in immunofluorescence assay (IFA) and PLA, and at 1:1,000 dilution in Western blot analysis. SC35 monoclonal antibody (Sigma-Aldrich, SAB4200725) was used at 1:1,000 dilution for IFA and Western blot. M2 anti-FLAG monoclonal antibody (Sigma-Aldrich, F1804) was used at 1:1,000 dilution. SON polyclonal antibody (GeneTex, GTX129778) was used at 1:500 dilution. Nucleolin monoclonal antibody (Invitrogen, 39-6400) was used at 1:500 dilution. hnRNP K polyclonal antibody (Invitrogen, PA5-27522) was used at 1:500 dilution. β-actin monoclonal antibody (Invitrogen, AM4302) was used at 1:5,000 dilution. NXF1 monoclonal antibody (Sigma-Aldrich, T1076) was used at 1:1,000 dilution. Aly/Ref monoclonal antibody (Sigma-Aldrich, A9979) was used at 1:500 dilution. SRSF1 monoclonal antibody (Invitrogen, 32-4600) was used at 1:500 dilution in Western blot analysis and 1:200 dilution in PLA. Anti–influenza A virion polyclonal antibody (Meridian Life Science) was used for detection of HA, NP, and M1 in Western blot analysis at 1:1,000 dilution. Anti-M2 antibody (Invitrogen, MA1-082) was used at 1:1,000 dilution. Alexa Fluor 488 goat anti-rabbit immunoglobulin G (IgG) and Alexa Fluor 546 goat anti-mouse IgG were used at 1:300 dilution. Enhanced chemiluminescent anti-mouse and anti-rabbit IgG, horseradish peroxidase–linked (GE Healthcare, NA931V, NA934V) were used at 1:10,000 dilution.

RNA Interference and Transfection. A pool of four siRNAs that target TAO2 (SMARTpool siRNA, Dharmacon) was used for RNA knockdown of TAO2. siRNAs were transfected into A549 cells using RNAiMAX (Invitrogen), according to the manufacturer's instructions. After 96 h, cells were fixed for imaging or lysed for biochemical approaches.

Western Blot. Western blot was performed as we previously described (30). Quantification of protein band intensity was obtained by generating a ratio of mean intensity over median intensity using Adobe Photoshop (CS4). Results were normalized to β-actin.

Immunofluorescence. Cells grown on coverslips were fixed for 15 min in 4% paraformaldehyde (PFA; Electron Microscopy Sciences) and then permeabilized for 5 min in phosphate-buffered saline (PBS) with 0.5% Triton X-100. After blocking (30 min, 5% bovine serum albumin; BSA), cells were immunostained for 1 h at 37 °C with the primary antibodies. The coverslips were washed three times with PBS and labeled with the secondary antibody for 1 h at 37 °C. Coverslips were then washed three times with PBS, stained with 1 μg/mL Hoechst 33258 (Molecular Probes Life Technologies) for 5 min, and briefly washed in PBS. Coverslips were mounted in ProLong Gold antifade reagent (Life Technologies).

Cell Fractionation. Cell fractionation was performed as previously described (43).

Immunoprecipitation and Mass Spectrometry. A549 cells were cultured in 10-cm plates for 24 h. Cells were then fractionated and the nuclear fraction was incubated in lysis buffer (50 mM Tris, pH 7.5, 150 mM NaCl, 1% Nonidet P-40, 0.1 mM Na_3VO_4, 1 mM NaF, 1 mM dithiothreitol, 1 mM ethylenediaminetetraacetate, 1 mM phenylmethylsulfonyl fluoride, 1× cOmplete protease inhibitor mixture, 10% glycerol) for 30 min at 4 °C and sonicated. The debris was removed by centrifugation at 12,000 rpm for 15 min. The supernatant was subjected to immunoprecipitation with protein A Sepharose (Sigma-Aldrich) preincubated with 5 μg anti-TAO2 antibody or rabbit IgG (Sigma-Aldrich) as negative control for 8 h at 4 °C. For experiments treated with RNasin RNase inhibitor (Roche), the reagent was added to a final concentration of 200 U/mL. For experiments treated with RNase A (Sigma-Aldrich), the enzyme was added to a final concentration of 1 μg/mL. After extensive washes with lysis buffer, the proteins were eluted by adding 2× sample buffer (63 mM Tris, 10% glycerol, 2% sodium dodecyl sulfate) and heating at 100 °C for 10 min. Samples were then subjected to mass spectrometry analysis as we have previously described (44). Protein abundances used to generate the heatmap shown in Fig. 2*A* were normalized using the heatmap.2 tool of the gplots package of the R Project.

Kinase Activity Assay. Purified TAO2 kinase (amino acids 1 to 314; Thermo Fisher Scientific) was incubated in the absence or presence of increasing concentrations of compound 2, as depicted in *SI Appendix*, Fig. S1*A*, and TAO2 kinase activity was measured using the Z′-LYTE activity assay (Thermo Fisher Scientific), according to the manufacturer's instructions.

RNA Purification and qRT-PCR. Total RNA was isolated from A549 cells with the RNeasy Plus Mini Kit (Qiagen) and 1 μg of total RNA was reverse-transcribed into complementary DNA (cDNA) by SuperScript II reverse transcriptase (Invitrogen) according to the manufacturer's instructions using 1 μM oligo (dT) as primers. cDNA was diluted with nuclease-free water at a ratio of 1:5 and 2 μL mixture was subjected to qPCR using SYBR Green I Master Mix and amplified by the LightCycler 480 qPCR System (Roche) with sequence-specific primers, as we previously described in detail (18). Data were normalized to β-actin mRNA levels. TAO2 qPCR primers were as follows: forward, 5′-GGGAAGCAGTCCAATGAGAAA-3′; reverse, 5′-CCGGTACTGAATGGTGTTGGG-3′. Primers for detection of additional cellular mRNAs are commercially available and were purchased from Bio-Rad (PrimePCR Assay System).

Proximity Ligation Assay. The Duolink In Situ Red Starter Kit Mouse/Rabbit (DUO92101, Sigma-Aldrich) was used to detect the interaction between TAO2 and SRSF1 in situ. Cells were seeded in 24-well plates with coverslips and cultured overnight. Coverslips were washed with PBS, fixed in 4% PFA for 15 min, and then blocked with Duolink blocking solution in a humid chamber for 1 h at 37 °C. The primary antibodies to detect TAO2 and SRSF1 were added to the coverslips and incubated for 1 h at 37 °C followed by washing with 1× wash buffer A (DUO82046 Sigma-Aldrich) twice and subsequently incubated with anti-mouse and anti-rabbit PLA probes (1:5 diluted in antibody diluents) for 1 h at 37 °C. The ligation-ligase solution was then added for 30 min followed by incubation with the amplification-polymerase solution for 100 min in a humidified chamber at 37 °C. Before imaging, coverslips were washed with 1× wash buffer B (DUO82048 Sigma-Aldrich) for 10 min twice and 0.01× wash buffer B for 1 min, and then mounted in Duolink in situ mounting medium containing DAPI.

Image Acquisition for PLA. Image series of fluorescent signals were acquired by spinning disk confocal microscopy (Nikon, CSU-W1 SoRa) using a 100× PLAN APO objective (glycerol immersion, numerical aperture 1.4). Images were recorded sequentially for each channel using a step size of 0.2 μm (total *z* size 12 μm). Acquired *z* stack images were blind-deconvolved using Autoquant X (Media Cybernetics).

Imaris-Assisted Image Analysis to Detect Cells, Nuclei, Nuclear Speckles, and TAO2–SRSF1 Complexes. The Imaris software package Cells module (Bitplane, version 9.8.2) was used to identify and create conventional 2D maximum-intensity projection and 3D isometric rendering images of the nucleus (chromatin), nuclear speckles (SC35 labeling), and PLA signal of the TAO2–SRSF1 complex display of confocal *z* stack fluorescence. First, nuclei (Hoechst) were segmented using an automated threshold (based on the intensity distribution histogram) in a 405-nm laser line. Identified nucleus populations were filtered to remove large nucleus aggregates (upper nucleus volume threshold and lower threshold to manually remove fragments of nuclei at the edges of the stack) using the Imaris surface tool. Next, nuclear speckles (SC35 marker) and PLA signal for TAO2 and SRSF1 interaction were identified in 488- and 561-nm laser lines, respectively, using the Imaris spot tool. The seed spot size used was 0.2 μm. For objective nuclear speckle center identification, automatic thresholds were used to filter raw spot quality.

smRNA-FISH, Imaging Quantification, and Statistics. These methods were described in detail in our previous publications (2, 18).

Viral Infection and Replication Assays. A549 cells transfected with control siRNA or siRNAs targeting TAO2 were infected with WSN at the indicated multiplicities of infection (MOIs) in infection media containing Eagle's minimal essential medium (ATCC), 10 mM Hepes (Gibco), 0.125% BSA (Gibco), and 0.5 mg/mL TPCK trypsin (Thermo Fisher Scientific). Cells were incubated with the virus for 1 h at 37 °C and washed briefly with PBS before incubation in fresh infection media. To assess viral replication, supernatants were serially diluted and added onto A549 cells growing on coverslips. Cells were then fixed with 4% PFA for 30 min at 8 h postinfection and subjected to immunofluorescence microscopy using an anti-NP primary antibody. Percent infection was quantified by dividing the NP-positive cells by the total number of cells, as we previously described (41).

RNA-Seq Data Analysis. Raw sequence data were trimmed using Trimmomatic (45). Quality control–filtered trimmed sequences were aligned to hg19 using STAR (46). All subsequent analysis was performed using R version 4.0.2 and Bioconductor 3.11 (47) in RStudio (R Core Team, 2020) (RStudio Team, 2020). The DESeq2 package was used for differential expression analysis between control and TAO2 knockdown, with Benjamini–Hochberg correction (false discovery rate < 0.05) (48). The volcano plot was generated using the EnhancedVolcano package (https://github.com/kevinblighe/EnhancedVolcano). Gene set enrichment analysis of the KEGG database was performed using the clusterProfiler package (49).

Data Availability. All study data are included in the article and/or supporting information.

ACKNOWLEDGMENTS. This work was supported by the following grants: NIH R01 AI154635 (to B.M.A.F.), NIH R01 AI125524 (to K.W.L., B.M.A.F., and M.H.C.), and Welch Foundation Grant I1243 (to M.H.C.). This work was also partly supported by the Center for Research of Influenza Pathogenesis and Transmission, National Institute of Allergy and Infectious Diseases (NIAID) Center of Excellence for Influenza Research and Response (Contract No. 75N93021C00014), and NIAID Grant U19AI135972 (to A.G.-S.), National Cancer Institute Grant U54 CA260560 Project 2 (to A.G.-S. and B.M.A.F.), and a Mary Kay Foundation International Postdoctoral Scholar Fellowship (to S.G.). J.W.S. holds the Southland Financial Corporation Distinguished Chair in Geriatrics and acknowledges grants CA070907 and CA264385.

Author affiliations: [a]Department of Cell Biology, University of Texas Southwestern Medical Center, Dallas, TX 75390; [b]Department of Molecular Biology, University of Texas Southwestern Medical Center, Dallas, TX 75390; [c]HHMI, University of Texas Southwestern Medical Center, Dallas, TX 75390; [d]Division of Molecular and Cellular Biology, National Institute of Child Health and Human Development, NIH, Bethesda, MD 20892; [e]Department of Biochemistry and Biophysics, University of Pennsylvania, Philadelphia, PA 19104; [f]Department of Microbiology, Icahn School of Medicine at Mount Sinai, New York, NY 10029; [g]Global Health and Emerging Pathogens Institute, Icahn School of Medicine at Mount Sinai, New York, NY 10029; [h]Division of Infectious Diseases, Department of Medicine, Icahn School of Medicine at Mount Sinai, New York, NY 10029; [i]The Tisch Cancer Institute, Icahn School of Medicine at Mount Sinai, New York, NY 10029; [j]Department of Pathology, Molecular and Cell-Based Medicine, Icahn School of Medicine at Mount Sinai, New York, NY 10029; [k]Department of Biophysics, University of Texas Southwestern Medical Center, Dallas, TX 75390; and [l]Department of Pharmacology, University of Texas Southwestern Medical Center, Dallas, TX 75390

1. A. P. Dias, K. Dufu, H. Lei, R. Reed, A role for TREX components in the release of spliced mRNA from nuclear speckle domains. *Nat. Commun.* **1**, 97 (2010).
2. A. Mor *et al.*, Influenza virus mRNA trafficking through host nuclear speckles. *Nat. Microbiol.* **1**, 16069 (2016).
3. J. Ule, B. J. Blencowe, Alternative splicing regulatory networks: Functions, mechanisms, and evolution. *Mol. Cell* **76**, 329–345 (2019).
4. M. G. Thompson, K. W. Lynch, Functional and mechanistic interplay of host and viral alternative splicing regulation during influenza infection. *Cold Spring Harb. Symp. Quant. Biol.* **84**, 123–131 (2019).
5. M. L. Yarbrough, M. A. Mata, R. Sakthivel, B. M. Fontoura, Viral subversion of nucleocytoplasmic trafficking. *Traffic* **15**, 127–140 (2014).
6. D. L. Spector, X. D. Fu, T. Maniatis, Associations between distinct pre-mRNA splicing components and the cell nucleus. *EMBO J.* **10**, 3467–3481 (1991).
7. I. A. Ilik *et al.*, SON and SRRM2 are essential for nuclear speckle formation. *eLife* **9**, e60579 (2020).
8. T. J. Stark, J. D. Arnold, D. H. Spector, G. W. Yeo, High-resolution profiling and analysis of viral and host small RNAs during human cytomegalovirus infection. *J. Virol.* **86**, 226–235 (2012).
9. T. Misteli, J. F. Cáceres, D. L. Spector, The dynamics of a pre-mRNA splicing factor in living cells. *Nature* **387**, 523–527 (1997).
10. C. Girard *et al.*, Post-transcriptional spliceosomes are retained in nuclear speckles until splicing completion. *Nat. Commun.* **3**, 994 (2012).
11. S. Masuda *et al.*, Recruitment of the human TREX complex to mRNA during splicing. *Genes Dev.* **19**, 1512–1517 (2005).
12. K. Wang *et al.*, Intronless mRNAs transit through nuclear speckles to gain export competence. *J. Cell Biol.* **217**, 3912–3929 (2018).
13. M. L. Shaw, P. Palese, "Orthomyxoviridae" in *Fields Virology*, D. M. Knipe, P. M. Howley, Eds. (Lippincott Williams & Wilkins, ed. 6, 2013), vol. **1**, pp. 1151–1185.
14. J. S. Rossman, X. Jing, G. P. Leser, R. A. Lamb, Influenza virus M2 protein mediates ESCRT-independent membrane scission. *Cell* **142**, 902–913 (2010).

15. S. Tripathi *et al.*, Meta- and orthogonal integration of influenza "OMICs" data defines a role for UBR4 in virus budding. *Cell Host Microbe* **18**, 723–735 (2015).
16. M. Gannagé *et al.*, Matrix protein 2 of influenza A virus blocks autophagosome fusion with lysosomes. *Cell Host Microbe* **6**, 367–380 (2009).
17. J. Ayllon, A. García-Sastre, The NS1 protein: A multitasking virulence factor. *Curr. Top. Microbiol. Immunol.* **386**, 73–107 (2015).
18. M. Esparza *et al.*, Chemical intervention of influenza virus mRNA nuclear export. *PLoS Pathog.* **16**, e1008407 (2020).
19. A. T. Piala *et al.*, Discovery of novel TAOK2 inhibitor scaffolds from high-throughput screening. *Bioorg. Med. Chem. Lett.* **26**, 3923–3927 (2016).
20. Z. Chen, M. H. Cobb, Regulation of stress-responsive mitogen-activated protein (MAP) kinase pathways by TAO2. *J. Biol. Chem.* **276**, 16070–16075 (2001).
21. M. Vanderkerken *et al.*, TAO-kinase 3 governs the terminal differentiation of NOTCH2-dependent splenic conventional dendritic cells. *Proc. Natl. Acad. Sci. U.S.A.* **117**, 31331–31342 (2020).
22. M. F. Wu, S. G. Wang, Human TAO kinase 1 induces apoptosis in SH-SY5Y cells. *Cell Biol. Int.* **32**, 151–156 (2008).
23. M. Richter *et al.*, Altered TAOK2 activity causes autism-related neurodevelopmental and cognitive abnormalities through RhoA signaling. *Mol. Psychiatry* **24**, 1329–1350 (2019).
24. F. C. de Anda *et al.*, Autism spectrum disorder susceptibility gene TAOK2 affects basal dendrite formation in the neocortex. *Nat. Neurosci.* **15**, 1022–1031 (2012).
25. C. Giacomini *et al.*, A new TAO kinase inhibitor reduces tau phosphorylation at sites associated with neurodegeneration in human tauopathies. *Acta Neuropathol. Commun.* **6**, 37 (2018).
26. J. Dopie, M. J. Sweredoski, A. Moradian, A. S. Belmont, Tyramide signal amplification mass spectrometry (TSA-MS) ratio identifies nuclear speckle proteins. *J. Cell Biol.* **219**, e201910207 (2020).
27. A. M. Jobbins *et al.*, Exon-independent recruitment of SRSF1 is mediated by U1 snRNP stem-loop 3. *EMBO J.* **41**, e107640 (2022).
28. Y. Xie, Y. Ren, Mechanisms of nuclear mRNA export: A structural perspective. *Traffic* **20**, 829–840 (2019).
29. P. L. Tsai *et al.*, Cellular RNA binding proteins NS1-BP and hnRNP K regulate influenza A virus RNA splicing. *PLoS Pathog.* **9**, e1003460 (2013).
30. K. Zhang *et al.*, Structural-functional interactions of NS1-BP protein with the splicing and mRNA export machineries for viral and host gene expression. *Proc. Natl. Acad. Sci. U.S.A.* **115**, E12218–E12227 (2018).
31. A. Karlas *et al.*, Genome-wide RNAi screen identifies human host factors crucial for influenza virus replication. *Nature* **463**, 818–822 (2010).
32. S. J. James *et al.*, MAPK phosphatase 5 expression induced by influenza and other RNA virus infection negatively regulates IRF3 activation and type I interferon response. *Cell Rep.* **10**, 1722–1734 (2015).
33. F. J. Barrat, M. K. Crow, L. B. Ivashkiv, Interferon target-gene expression and epigenomic signatures in health and disease. *Nat. Immunol.* **20**, 1574–1583 (2019).
34. A. Dukhovny *et al.*, A CRISPR activation screen identifies genes that protect against Zika virus infection. *J. Virol.* **93**, e00211-19 (2019).
35. H. V. Mears, T. R. Sweeney, Better together: The role of IFIT protein-protein interactions in the antiviral response. *J. Gen. Virol.* **99**, 1463–1477 (2018).
36. C. Ehrhardt, S. Ludwig, A new player in a deadly game: Influenza viruses and the PI3K/Akt signalling pathway. *Cell. Microbiol.* **11**, 863–871 (2009).
37. S. K. Kuss-Duerkop *et al.*, Influenza virus differentially activates mTORC1 and mTORC2 signaling to maximize late stage replication. *PLoS Pathog.* **13**, e1006635 (2017).
38. M. D. Turner, B. Nedjai, T. Hurst, D. J. Pennington, Cytokines and chemokines: At the crossroads of cell signalling and inflammatory disease. *Biochim. Biophys. Acta* **1843**, 2563–2582 (2014).
39. T. Katsuyama, V. R. Moulton, Splicing factor SRSF1 is indispensable for regulatory T cell homeostasis and function. *Cell Rep.* **36**, 109339 (2021).
40. T. Katsuyama, H. Li, S. M. Krishfield, V. C. Kyttaris, V. R. Moulton, Splicing factor SRSF1 limits IFN-γ production via RhoH and ameliorates experimental nephritis. *Rheumatology (Oxford)* **60**, 420–429 (2021).
41. K. White *et al.*, Aryl sulfonamide inhibits entry and replication of diverse influenza viruses via the hemagglutinin protein. *J. Med. Chem.* **64**, 10951–10966 (2021).
42. V. Aksenova *et al.*, Nucleoporin TPR is an integral component of the TREX-2 mRNA export pathway. *Nat. Commun.* **11**, 4577 (2020).
43. Y. Wang, W. Zhu, D. E. Levy, Nuclear and cytoplasmic mRNA quantification by SYBR Green based real-time RT-PCR. *Methods* **39**, 356–362 (2006).
44. K. Zhang *et al.*, Nsp1 protein of SARS-CoV-2 disrupts the mRNA export machinery to inhibit host gene expression. *Sci. Adv.* **7**, eabe7386 (2021).
45. A. M. Bolger, M. Lohse, B. Usadel, Trimmomatic: A flexible trimmer for Illumina sequence data. *Bioinformatics* **30**, 2114–2120 (2014).
46. A. Dobin *et al.*, STAR: Ultrafast universal RNA-seq aligner. *Bioinformatics* **29**, 15–21 (2013).
47. W. Huber *et al.*, Orchestrating high-throughput genomic analysis with Bioconductor. *Nat. Methods* **12**, 115–121 (2015).
48. M. I. Love, W. Huber, S. Anders, Moderated estimation of fold change and dispersion for RNA-seq data with DESeq2. *Genome Biol.* **15**, 550 (2014).
49. G. Yu, L. G. Wang, Y. Han, Q. Y. He, clusterProfiler: An R package for comparing biological themes among gene clusters. *OMICS* **16**, 284–287 (2012).